

Cite this: *Phys. Chem. Chem. Phys.*, 2012, **14**, 7162–7169

www.rsc.org/pccp

Poly(2,5-bis(2-octyldodecyl)-3,6-di(furan-2-yl)-2,5-dihydro-pyrrolo[3,4-*c*]-pyrrole-1,4-dione-*co*-thieno[3,2-*b*]thiophene): a high performance polymer semiconductor for both organic thin film transistors and organic photovoltaics†

Yuning Li,^{*ab} Prashant Sonar,^b Samarendra P. Singh,^{‡b} Zi En Ooi,^b Erica S. H. Lek^b and Melissa Q. Y. Loh^b

Received 23rd March 2012, Accepted 26th March 2012

DOI: 10.1039/c2cp40937b

A new diketopyrrolopyrrole (DPP)-containing donor–acceptor polymer, poly(2,5-bis(2-octyldodecyl)-3,6-di(furan-2-yl)-2,5-dihydro-pyrrolo[3,4-*c*]pyrrole-1,4-dione-*co*-thieno[3,2-*b*]thiophene) (PDBF-*co*-TT), is synthesized and studied as a semiconductor in organic thin film transistors (OTFTs) and organic photovoltaics (OPVs). High hole mobility of up to $0.53 \text{ cm}^2 \text{ V}^{-1} \text{ s}^{-1}$ in bottom-gate, top-contact OTFT devices is achieved owing to the ordered polymer chain packing and favoured chain orientation, strong intermolecular interactions, as well as uniform film morphology of PDBF-*co*-TT. The optimum band gap of 1.39 eV and high hole mobility make this polymer a promising donor semiconductor for the solar cell application. When paired with a fullerene acceptor, PC₇₁BM, the resulting OPV devices show a high power conversion efficiency of up to 4.38% under simulated standard AM1.5 solar illumination.

Introduction

Conjugated polymers comprising alternating electron donor (D) and acceptor (A) units are of rapidly growing interest since many of them are excellent semiconductor materials for organic thin film transistors (OTFTs)^{1–13} and organic photovoltaics (OPVs).^{13–17} 2,5-Dihydro-pyrrolo[3,4-*c*]pyrrole-1,4-dione or more commonly diketopyrrolopyrrole (DPP) is one of the most important electron accepting building blocks for high mobility polymer semiconductors.^{4–10} When coupled with appropriate electron donors, the resulting DPP-containing DA polymers have strong intermolecular D–A interactions, which could shorten the π – π stacking distance to facilitate charge hopping between polymer chains. On the other hand, fused aromatic rings that can bring about strong π – π interactions and increase π -stacking overlap areas are also very useful building blocks for constructing π -conjugated polymers with highly

efficient charge transport characteristics.^{18–23} Among them, thieno[3,2-*b*]thiophene (TT) is an excellent building block and several TT-containing polymers have shown high charge transport mobility in OTFTs.^{18,19} Previously we reported a polymer, PDBT-*co*-TT (Fig. 1), comprising DPP and TT blocks which are linked with thiophene units. PDBT-*co*-TT showed high hole mobility of up to $0.94 \text{ cm}^2 \text{ V}^{-1} \text{ s}^{-1}$ in OTFTs, owing to the strong intermolecular interactions.⁴ Later, this polymer was also found to be an excellent ambipolar semiconductor, exhibiting a high hole mobility of $1.18 \text{ cm}^2 \text{ V}^{-1} \text{ s}^{-1}$ and an electron mobility of $1.86 \text{ cm}^2 \text{ V}^{-1} \text{ s}^{-1}$ in OTFT devices which were fabricated at high temperature using modified

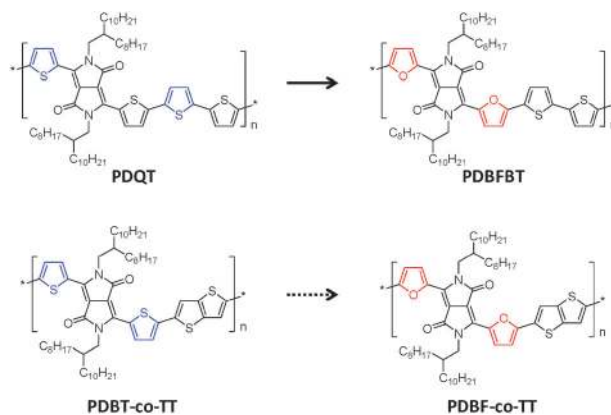


Fig. 1 Structures of some DPP-containing D–A polymers.

^a Department of Chemical Engineering/Waterloo Institute for Nanotechnology (WIN), University of Waterloo, 200 University Ave West, Waterloo, ON, Canada, N2L 3G1. E-mail: yuning.li@uwaterloo.ca; Fax: +1-519-888-4347; Tel: +1-519-888-4567 ext. 31105

^b Institute of Materials Research and Engineering (IMRE) and the Agency for Science, Technology and Research (A*STAR), 3 Research Link, Singapore, 117602, Singapore

† Electronic supplementary information (ESI) available: Gel-permeation chromatography (GPC) and differential scanning calorimetry (DSC) data. See DOI: 10.1039/c2cp40937b

‡ Current address: School of Natural Sciences, Shiv Nadar University, Gautam Buddh Nagar, U.P. 203207, India.

contacts.²⁴ Recently, we found that a DPP-containing polymer, PDBFBT (Fig. 1), which was incorporated with furan, instead of thiophene, exhibited much improved hole mobility of up to $1.54 \text{ cm}^2 \text{ V}^{-1} \text{ s}^{-1}$,⁶ as compared with its thiophene counterpart PDQT (Fig. 1) that showed a hole mobility of $0.97 \text{ cm}^2 \text{ V}^{-1} \text{ s}^{-1}$.⁵ Inspired by the high performance of PDBFBT, here we use furan to link the DPP and TT units to form poly(2,5-bis(2-octyldodecyl)-3,6-di(furan-2-yl)-2,5-dihydro-pyrrolo[3,4-*c*]pyrrole-1,4-dione-*co*-thieno[3,2-*b*]thiophene) (PDBF-*co*-TT) (Fig. 1), which is a structural analog of PDBT-*co*-TT. The optical properties, molecular ordering, thin film morphology, as well as the charge transport properties of this new polymer are systematically investigated. Our results show that PDBF-*co*-TT is a high-performing p-type semiconductor material for organic thin film transistors with high hole mobility of up to $\sim 0.53 \text{ cm}^2 \text{ V}^{-1} \text{ s}^{-1}$. In addition to its high hole mobility, PDBF-*co*-TT has a small band gap of $\sim 1.39 \text{ eV}$, making this polymer an ideal absorber and donor material for OPVs. Power conversion efficiency of up to 4.38% is achieved when this polymer is paired with PC₇₁BM, to be used as an active layer in OPV devices.

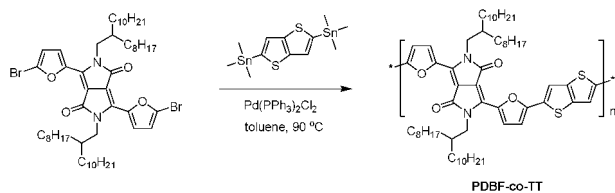
Results and discussion

Synthesis and characterization of PDBF-*co*-TT

Polymer PDBF-*co*-TT was synthesized according to Scheme 1. Stille coupling polymerization of 3,6-bis(5-bromo-2-furanyl)-2,5-bis(2-octyldodecyl)-2,5-dihydro-pyrrolo[3,4-*c*]pyrrole-1,4-dione and 2,5-bis(trimethylstannyl)bithiophene was conducted in toluene at 90 °C under an argon atmosphere in the presence of a catalyst, Pd(PPh₃)₂Cl₂. This reaction afforded PDBF-*co*-TT in a high isolated yield ($\sim 98\%$) after purification with Soxhlet extraction using methanol, acetone, and hexane. PDBF-*co*-TT showed much improved solubility in THF, chloroform, and several other common organic solvents as compared with its thiophene counterpart, PDBT-*co*-TT.⁴ The number average molecular weight (M_n) and polydispersity index (PDI, M_w/M_n) of PDBF-*co*-TT were determined to be 132 kDa and 2.63, respectively, with GPC using THF as an eluent and polystyrene as standard.

As shown in Fig. 2, PDBF-*co*-TT displays a maximum absorption (λ_{max}) at 797 nm with a clear vibronic shoulder at 723 nm in chloroform. The polymer thin film shows a similar λ_{max} at 794 nm, but the absorption profile becomes much broader and strongly absorbs from 600 nm to 850 nm. The vibronic shoulder ($\sim 712 \text{ nm}$) remains prominent, but more intensified compared with the shoulder observed in the solution spectrum. The optical band gap estimated from the absorption cutoff wavelength is 1.39 eV, which is larger than that (1.23 eV) of PDBT-*co*-TT.⁴

PDBF-*co*-TT showed reversible oxidative and reductive cycles during cyclic voltammetric (CV) scans (Fig. 3). The electrical response in the oxidative sweep is significantly stronger than



Scheme 1 Synthesis of PDBF-*co*-TT via Stille coupling polymerization.

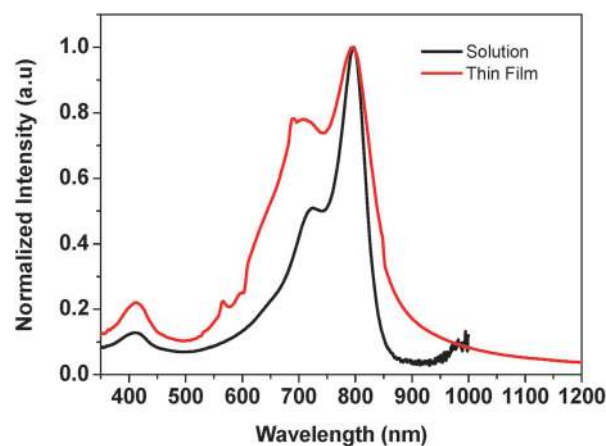


Fig. 2 UV-vis-NIR absorption spectra of PDBF-*co*-TT in CHCl₃ solution (black) and in thin film (red) on a glass substrate.

that in the reductive sweep, indicating that this polymer favors hole transport over electron transport. The oxidation and reduction onset potentials are +0.93 V and -0.98 V, respectively. The band gap calculated from the CV results is 1.91 eV, which is considerably larger than the optical band gap (1.39 eV) obtained from the thin film UV-vis-NIR spectrum. This is considered due to the exciton binding energy of this polymer as observed for other semiconductor polymers.^{25,26} Since ferrocene showed an oxidation onset potential of +0.45 V under the same experimental conditions, the HOMO energy level of PDBF-*co*-TT is calculated to be 5.28 eV, based on the HOMO (4.8 eV) of ferrocene. (Calculation using $E_{\text{HOMO}} = 4.4 \text{ eV} + E_{\text{onset}}$ ²⁷⁻²⁹ gave a similar value: $E_{\text{HOMO}} = 5.33 \text{ eV}$.) The LUMO energy level of PDBF-*co*-TT is thus calculated to be 3.89 eV, by using the E_{HOMO} (5.28 eV) obtained from the CV results and the band gap (1.39 eV) obtained from the UV-vis measurement.

The crystallinity and molecular organization of spin-coated PDBF-*co*-TT thin films on octyltrichlorosilane (OTS)-treated Si/SiO₂ wafer substrates were characterized by using an X-ray diffractometer (XRD). The non-annealed polymer thin film showed a very weak diffraction peak at $2\theta = 4.56^\circ$ (Fig. 4). For the thin film annealed at 100 °C, this primary peak intensified significantly. Further increasing the annealing temperature to 140 °C, the primary peak further increased and the secondary

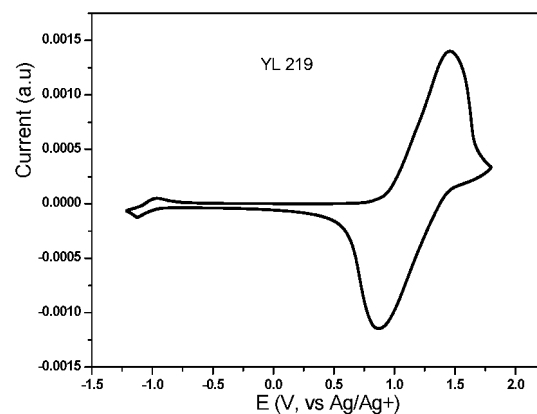


Fig. 3 The first cyclic voltammogram (CV) redox cycle of a PDBF-*co*-TT thin film.

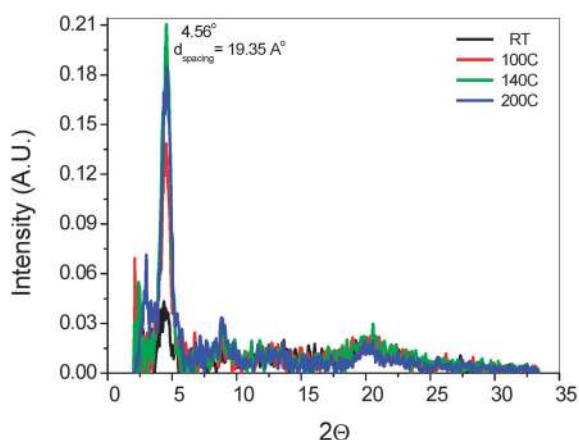


Fig. 4 X-ray diffraction (XRD) data obtained from spin-coated PDBF-*co*-TT thin films (~ 35 nm) on OTS treated SiO₂/Si substrates annealed at different temperatures.

peak at $2\theta = 7.16^\circ$ started to appear. When the annealing temperature was increased to 200 °C, no obvious improvements in crystallinity were observed. The intensity of the broad peak at $\sim 20^\circ$ remained nearly constant, which might be due to the short-range ordering in the amorphous regions in the thin films. These XRD patterns resemble many other conjugated polymers such as P3HT, which were determined to reflect a layer-by-layer lamellar polymer chain packing structure.³⁰ Since there is no discernible peak corresponding to the π - π stacking distance, it can be concluded that the polymer chains in the spin coated thin films predominantly adopted an edge-on chain orientation. Polymer chains aligned in this manner on the substrate are most favored for the charge transport in OTFT devices.³⁰

The thin film surface morphology of PDBF-*co*-TT was visualized by using the atomic force microscopy (AFM) technique. The non-annealed sample showed a smooth surface comprising long fine fibrils (Fig. 5). Once the thin film was annealed to 100 °C, the fibrils became thicker and shorter. Further increasing the annealing temperature to 140 and 200 °C, the size and the shape of the fibrils remained similar, but the contours of the fibrils became clearer, indicating the increased crystallinity of the polymer thin film. All the AFM images showed well-interconnected networks without large grain boundaries, which is beneficial for the charge hopping between crystalline domains.^{4,5}

Evaluation of PDBF-*co*-TT in OTFT devices

PDBF-*co*-TT was evaluated as a channel semiconductor in bottom-gate, top-contact OTFT devices. An OTS-treated Si/SiO₂ wafer was used as substrate to construct the device. The heavily *n*+ -doped Si base functioned as the gate electrode, whereas the ~ 200 nm thermally grown SiO₂ top layer was used as the dielectric layer. A ~ 35 nm-thick PDBF-*co*-TT film was deposited on top of the OTS-treated SiO₂ layer by spin-coating a PDBF-*co*-TT solution in chloroform (8 mg mL⁻¹), followed by optional thermal annealing on a hot plate at 140 or 200 °C under dry nitrogen in a glove box. Subsequently, the substrate with the polymer layer was transferred to a high vacuum thermal evaporator to deposit the source and drain top contacts

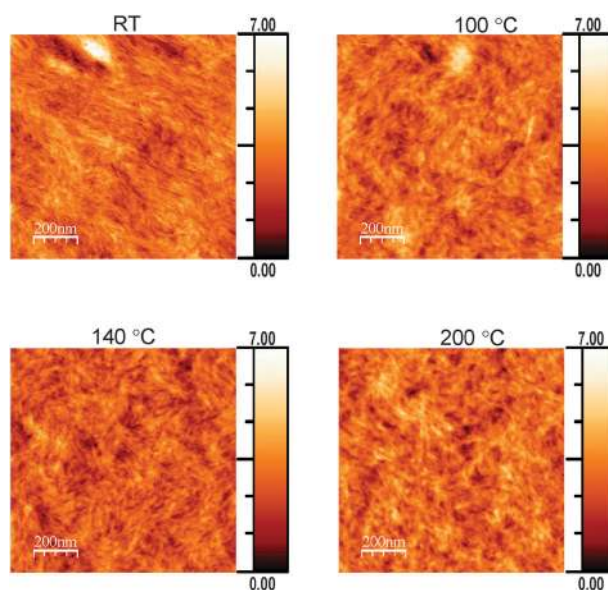


Fig. 5 Atomic Force Microscopy (AFM) data obtained from spin-coated PDBF-*co*-TT thin films (~ 35 nm) on OTS treated SiO₂/Si substrates annealed at different temperatures.

through a shadow mask with the channel dimensions of 100 micron (L) \times 1 mm (W). The field effect characteristics were then analyzed under dry nitrogen in a glove box.

As shown in Fig. 6 and 7, the device having the non-annealed PDBF-*co*-TT film showed characteristic output and transfer curves of a typical p-channel field effect transistor. In the accumulation mode, the mobility extracted from the saturation regime is 0.34 cm² V⁻¹ s⁻¹ with a high current on-to-off ratio ($I_{ON/OFF}$) of $\sim 10^6$. The threshold voltage (V_{TH})

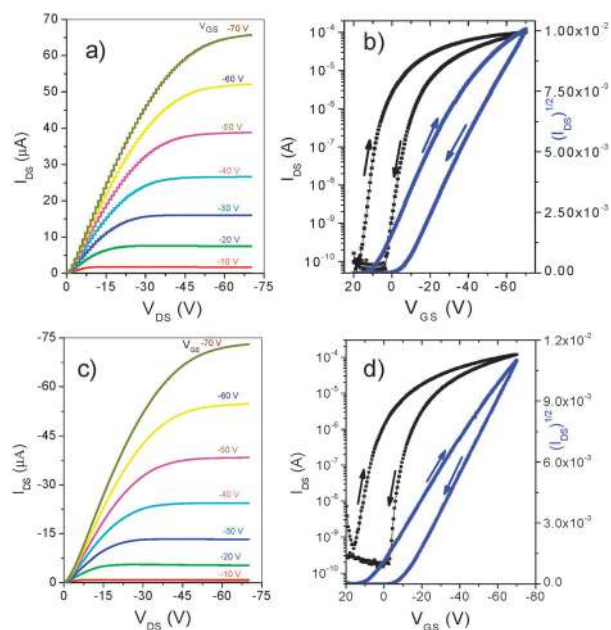


Fig. 6 The output (left: $V_G = 0$ V to -70 V) and transfer (right: $V_{DS} = -70$ V) characteristics of an OTFT device with PDBF-*co*-TT thin films without annealing (a and b) and annealed at 100 °C for 15 min (c and d). Device dimensions: channel length (L) = 100 μ m; channel width (W) = 1 mm.

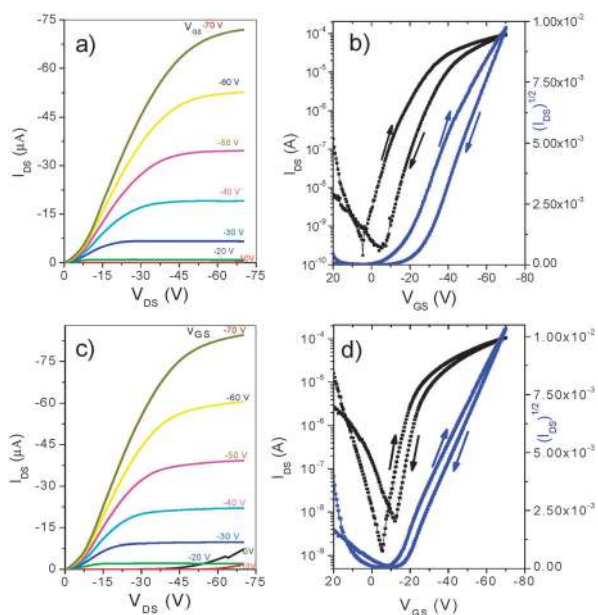


Fig. 7 The output (left: $V_G = 0$ V to -70 V) and transfer (right: $V_{DS} = -70$ V) characteristics of an OTFT device with PDBF-*co*-TT thin films annealed at 140 °C (a and b) and 200 °C for 15 min (c and d). Device dimensions: channel length (L) = 100 μm ; channel width (W) = 1 mm.

is 8.7 V, which indicates that p-doping or electron trapping²⁴ in the semiconductor might exist. The reverse voltage sweep in the hole accumulation mode showed a hysteresis with a ΔV_{TH} ($V_{TH,forward} - V_{TH,backward}$) = 12.4 V, which is commonly observed for most polymer semiconductor based OTFTs. The causes for the hysteresis are considered to be surface traps^{31–33} and/or conformation changes of the polymer chains under an electrical bias.³⁴ The OTFT device having a PDBF-*co*-TT film annealed at 100 °C displayed a slightly decreased mobility of 0.25 $\text{cm}^2 \text{V}^{-1} \text{s}^{-1}$. The V_{TH} shifted slightly to 6.6 V in the negative direction. A large hysteresis ($\Delta V_{TH} = 16.8$ V) is still observed. When the polymer film was annealed at 140 °C, the mobility was increased notably to 0.49 $\text{cm}^2 \text{V}^{-1} \text{s}^{-1}$. A negative threshold voltage ($V_{TH} = -15.5$ V) was shown, indicating that p-doping or electron trapping effect was completely removed by thermal annealing at this temperature. The hysteresis effect is somehow decreased ($\Delta V_{TH} = 10.3$ V). Interestingly, in the positive gate voltage region ($V_{GS} = 0$ V– $+20$ V), a slight electron transport behavior was observed. When the annealing temperature was increased further to 200 °C, the OTFT device showed a marginal increase in mobility (0.53 $\text{cm}^2 \text{V}^{-1} \text{s}^{-1}$) and a slight decrease in V_{TH} (-12.6 V). The hysteresis ($\Delta V_{TH} = 4.4$ V) is significantly reduced, which might be due to elimination of the structural disorder and traps in this high-temperature annealed polymer thin film. This device showed even more prominent electron transport characteristics in the positive gate voltage region ($V_{GS} = 0$ V– $+20$ V). The increasingly pronounced ambipolar transport behaviour with increasing annealing temperature was also recently observed for PDBT-*co*-TT,²⁴ the structural analogue of PDBF-*co*-TT. This is possibly attributed to the removal of electron trapping impurities at a high annealing temperature. The effect of thermal annealing on the electron

trapping becomes more obvious if the hole switch-on voltage ($V_{switch-on}^{hole}$) is considered. As the annealing temperature is increased from room temperature (non-annealed) to 100 , 140 , and 200 °C, the $V_{switch-on}^{hole}$ progressively moved towards the negative V_{GS} direction from $+18.8$ V to $+16.7$ V, $+4.6$ V, and -5.3 V. When the device was tested in the electron enhancement mode ($V_{GS} = -20$ V to $+70$ V and $V_{DS} = 0$ V to $+70$ V), however, no saturation characteristics were observed in electron enhancement mode. Therefore PDBF-*co*-TT is predominantly a hole transport material by nature.

Organic solar cells based on PDBF-*co*-TT and PC₇₁BM

DPP-containing D–A polymers have been recently extensively investigated as efficient donor materials for OPVs.^{9,35–39} The optical band gap (~ 1.39 eV) of PDBF-*co*-TT is close to the ideal band gap for optimum power conversion of sunlight, while its relatively low-lying HOMO and LUMO energy levels would lower the energy loss during the electron transfer and achieve a high open circuit voltage (V_{OC}).^{14,15,40,41} Additionally, the high hole mobility of this polymer would be beneficial for hole transport to the anode to minimize charge recombination for achieving a high fill factor (FF). In this study, we used PDBF-*co*-TT as an electron donor material to pair with a widely used electron acceptor, PC₇₁BM, to form a blend bulk-heterojunction layer in OPV devices. Indium-doped tin oxide (ITO) glass was used as both the anode and the substrate support to construct the OPV devices. Prior to use, the properly cleaned ITO glass was deposited with a layer of PEDOT:PSS (~ 40 nm) on the top of ITO layer by spin coating a Clevis 4083 PEDOT:PSS solution at 2000 rpm and then annealed at 140 °C on a hotplate under nitrogen. An active blend film of PDBF-*co*-TT and PC₇₁BM with a certain weight ratio was deposited on the substrate by spin coating a semiconductor solution in a mixture of chloroform and *o*-dichlorobenzene ($4 : 1$ by volume) with a solid concentration of 24 mg mL^{-1} . Finally a layer of aluminium as a cathode was thermally evaporated on top of the semiconductor layer through a shadow mask, forming a square device with an area of approximately 9 mm^2 .

The first batch of devices were based on a permutation of three blend compositions (the donor-to-acceptor ratio (D : A) = $1 : 1$, $1 : 2$, and $1 : 3$) and three different additive conditions (no additive, 1-chloro-naphthalene (CNp), and 1,8-diiodooctane (DIO)). Solvent additives are known to be able to improve the OPV performance, often dramatically.^{42–45} Table 1 summarizes the performance of the most efficient cell from each process combination.

Without any solvent additive, the OPV devices for all three blend compositions (D : A = $1 : 1$, $1 : 2$, and $1 : 3$) showed very low short circuit current densities ($J_{SC} \leq 1.72$ mA cm^{-2}) and low power conversion efficiencies (PCE $\leq 0.74\%$). It was found that the FF increases with an increasing amount of PC₇₁BM (D : A from $1 : 1$ to $1 : 3$). This might be due to the electron mobility of PC₇₁BM being lower than the hole mobility of PDBF-*co*-TT, which results in unbalanced hole and electron transports when D : A is $1 : 1$. However, the increase in FF is marginal and J_{SC} starts to fall when the D : A ratio is decreased to $1 : 3$, probably due to the reduced amount

Table 1 Figures of merit of PDBF-*co*-TT:PC₇₁BM-based OPV devices with varied D : A ratios and different solvent additives. Data are from the best-performing devices chosen from 9 devices for each process combination. Data in parentheses are average values and standard deviations from the top 4 performing devices

| D : A ratio | Solvent additive | $J_{SC}/\text{mA cm}^{-2}$ | V_{OC}/V | FF | PCE (%) |
|-------------|------------------|----------------------------|--------------------|--------------------|--------------------|
| 1 : 1 | None | 1.3 (1.2 ± 0.1) | 0.71 (0.71 ± 0.01) | 0.45 (0.45 ± 0.00) | 0.42 (0.39 ± 0.03) |
| | CNp 1% (vol) | 3.7 (3.4 ± 0.2) | 0.68 (0.69 ± 0.01) | 0.40 (0.40 ± 0.00) | 1.0 (0.94 ± 0.05) |
| | DIO 1% (vol) | 12.1 (11.6 ± 1.0) | 0.67 (0.63 ± 0.06) | 0.42 (0.40 ± 0.04) | 3.4 (3.0 ± 0.8) |
| 1 : 2 | None | 1.7 (1.6 ± 0.1) | 0.70 (0.71 ± 0.01) | 0.61 (0.62 ± 0.01) | 0.74 (0.72 ± 0.02) |
| | CNp 1% (vol) | 3.2 (3.0 ± 0.1) | 0.70 (0.70 ± 0.01) | 0.50 (0.52 ± 0.02) | 1.1 (1.1 ± 0.00) |
| | DIO 1% (vol) | 11.3 (11.4 ± 0.5) | 0.68 (0.67 ± 0.01) | 0.52 (0.52 ± 0.04) | 4.0 (3.9 ± 0.1) |
| 1 : 3 | None | 1.4 (1.3 ± 0.1) | 0.73 (0.72 ± 0.01) | 0.62 (0.62 ± 0.00) | 0.64 (0.60 ± 0.04) |
| | CNp 1% (vol) | 2.0 (1.9 ± 0.1) | 0.72 (0.72 ± 0.01) | 0.63 (0.63 ± 0.00) | 0.92 (0.84 ± 0.2) |
| | DIO 1% (vol) | 9.0 (8.6 ± 0.3) | 0.68 (0.69 ± 0.01) | 0.61 (0.62 ± 0.04) | 3.76 (3.6 ± 0.2) |

of PDBF-*co*-TT that causes weaker light absorption and poorer connectivity of the donor phase. A quite high V_{OC} of up to 0.73 V was obtained, which originated from the low-lying HOMO energy level (~ 5.28 eV) of PDBF-*co*-TT.

When 1% CNp was used as a solvent additive, a notable increase in J_{SC} (up to 3.66 mA cm^{-2}) was observed, while both V_{OC} and FF decreased slightly. With the use of 1% CNp solvent additive, the highest PCE of 1.10% was obtained for the blend composition of D : A = 1 : 2. In all blend compositions, addition of 1% DIO in the solvent mixture was found to improve the cell performance significantly. The best performance was observed for the device using a blend composition of D : A = 1 : 2, which showed a high J_{SC} of 11.3 mA cm^{-2} , ~ 6.6 times of that (1.72 mA cm^{-2}) of the best-performing device fabricated without any solvent additive. This device showed a high PCE of 4.03%, although its V_{OC} and FF are slightly lower than those for the devices without a solvent additive or with 1% CNp. Encouraged by the high PCE for the device fabricated using a blend of D : A = 1 : 2 and DIO as a solvent additive, we further optimized the fabrication process by varying the spin coating speed (1500, 2500 and 4000 rpm) and the DIO content (0.5, 1, and 2% by volume). The performance of the most efficient cells from each set of fabrication parameters is summarized in Table 2.

This set of experiments shows clearly that the FF improves as the spin coating speed increases. This could be accounted for by the decreasing thickness of the active blend layer with increasing spin coating speed; a thinner active layer would suppress charge recombination (increased FF). On the other hand, the influence of the spin coating speed on the J_{SC} is

insignificant. The effects of the DIO additive content within the range of 0.5–2% were found to be insignificant. The highest PCE of 4.38% was achieved for the device fabricated at a spin speed of 4000 rpm using 0.5% of DIO.

The inset of Fig. 8 shows the external quantum efficiency (EQE) of the best OPV device in this study, measured under low-intensity monochromatic light. The EQE spectrum indicates that the PDBF-*co*-TT:PC₇₁BM blend is photo-active between 300 and 900 nm, in a good agreement with the absorption profile of the PDBF-*co*-TT (Fig. 2) and PC₇₁BM. Fig. 8 also shows the current density–voltage curves of the same device measured in dark and irradiated under a simulated AM1.5 light source. We used the EQE spectrum to calculate a spectral mismatch factor for an appropriate solar simulator light level for the light source calibration.⁴⁶ As an additional verification step, it is prudent to calculate the theoretical J_{SC} from the EQE spectrum by integrating its convolution with the AM1.5 spectrum. The measured J_{SC} agrees very well with the calculated value, suggesting that under short-circuit conditions, losses associated with high photogenerated carrier densities are minimal in this device.

The OPV performance observed for PDBF-*co*-TT is much better than that of its thiophene analogue, PDBT-*co*-TT, which was reported to show a maximum PCE of $\sim 1.6\%$.³⁶ Several other furan-containing DPP-based polymers have also shown improved efficiencies in comparison to their thiophene counterparts.^{35,37–39} The slightly wider band gap and lower HOMO levels of the furan-containing polymers might be beneficial for their OPV performance. Another possible reason is that the furan-containing DPP polymers have better

Table 2 Figures of merit of PDBF-*co*-TT:PC₇₁BM-based OPV devices with a D : A ratio of 1 : 2 (by volume) and varied spin coating speed and amount of DIO. Data are from the best-performing devices chosen from 9 devices for each process combination. Data in parentheses are average values and standard deviations from the top 4 performing devices

| Spin speed/rpm | DIO content (%) | $J_{SC}/\text{mA cm}^{-2}$ | V_{OC}/V | FF | PCE (%) |
|----------------|-----------------|----------------------------|--------------------|--------------------|-----------------|
| 1500 | 0.5 | 10.7 (11.1 ± 0.4) | 0.68 (0.68 ± 0.01) | 0.55 (0.52 ± 0.02) | 4.0 (3.9 ± 0.1) |
| | 1 | 11.1 (11.5 ± 0.5) | 0.67 (0.67 ± 0.00) | 0.52 (0.49 ± 0.02) | 3.9 (3.8 ± 0.1) |
| | 2 | 11.4 (11.7 ± 0.3) | 0.67 (0.67 ± 0.00) | 0.51 (0.48 ± 0.02) | 3.9 (3.8 ± 0.1) |
| 2500 | 0.5 | 10.9 (11.0 ± 0.3) | 0.68 (0.67 ± 0.01) | 0.58 (0.55 ± 0.03) | 4.3 (4.1 ± 0.3) |
| | 1 | 10.4 (10.8 ± 0.4) | 0.67 (0.65 ± 0.03) | 0.56 (0.52 ± 0.03) | 3.9 (3.7 ± 0.3) |
| | 2 | 12.1 (11.2 ± 0.8) | 0.67 (0.67 ± 0.01) | 0.52 (0.52 ± 0.02) | 4.2 (4.0 ± 0.2) |
| 4000 | 0.5 | 10.8 (10.9 ± 0.3) | 0.69 (0.68 ± 0.01) | 0.59 (0.56 ± 0.03) | 4.4 (4.2 ± 0.2) |
| | 1 | 10.2 (10.5 ± 0.4) | 0.69 (0.68 ± 0.01) | 0.60 (0.57 ± 0.03) | 4.2 (4.1 ± 0.1) |
| | 2 | 11.4 (11.2 ± 0.3) | 0.68 (0.68 ± 0.00) | 0.54 (0.55 ± 0.02) | 4.2 (4.1 ± 0.1) |

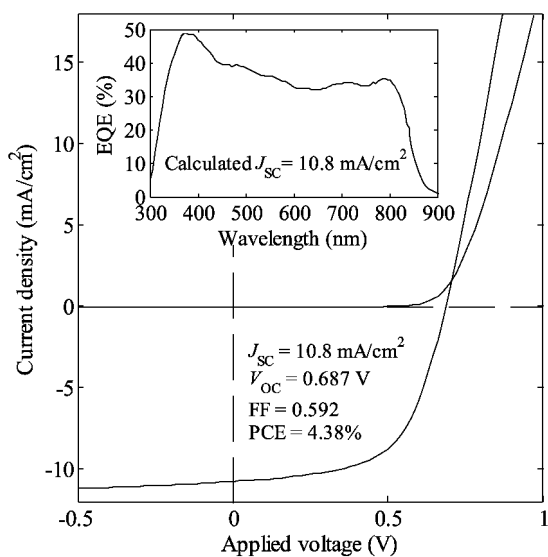


Fig. 8 Current density–voltage curves of the best PDBF-*co*-TT:PC₇₁BM-based solar cell under dark and simulated AM1.5 solar illumination conditions. The inset is the external quantum efficiency (EQE) spectrum under low light levels.

solubility in general than their corresponding thiophene-based polymers,³⁷ which facilitate the formation of higher quality polymer blend layers.

Experimental

Instrumentations and materials

Gel permeation chromatography (GPC) measurements were conducted on a Waters 2690 System using tetrahydrofuran (THF) as eluent and polystyrene as standard at a column temperature of 40 °C. UV-vis-NIR spectra were recorded on a Shimadzu UV 2501PC Spectrophotometer in solution (chloroform) or on thin films on quartz glass substrates. Cyclic voltammetry (CV) measurements were performed using an Ecochimie PGSTAT30 Autolab potentiostat in 0.1 M tetrabutylammonium hexafluorophosphate (TBAPF₆) in dry acetonitrile at a sweep rate of 100 mV s⁻¹ under dry nitrogen in a glove box. An Ag/AgCl electrode in 3 M KCl, a Pt wire, and a Pt foil were used as the reference electrode, counter electrode, and working electrode, respectively, where the polymer sample was coated from a dilute solution in chloroform on the Pt foil. Ferrocene, which has a HOMO energy level of 4.8 eV,^{47–49} was used as an external reference. The HOMO energy level of PDBF-*co*-TT was calculated by comparing its onset oxidation potential with that of ferrocene. Differential scanning calorimetry (DSC) measurements were carried out under nitrogen on a TA Instrument DSC Q100 instrument at a scanning rate of 10 °C min⁻¹. X-ray diffraction (XRD) measurements were performed on a PANalytical X'PERT PRO system using a Cu K_α source ($\lambda = 1.5418 \text{ \AA}$). The polymer thin films for the XRD measurements were deposited on octyltrichlorosilane (OTS)-treated Si/SiO₂ wafer substrates. 3,6-Bis(5-bromo-2-furanyl)-2,5-bis(2-octyldodecyl)-2,5-dihydro-pyrrolo[3,4-*c*]pyrrole-1,4-dione⁶ and 2,5-bis(trimethylstannyl)-thieno[3,2-*b*]thiophene¹⁸ were prepared according to the literature methods.

Synthesis of poly(2,5-bis(2-octyldodecyl)-3,6-di(furan-2-yl)-2,5-dihydro-pyrrolo[3,4-*c*]pyrrole-1,4-dione-*co*-thieno[3,2-*b*]thiophene) (PDBF-*co*-TT)

3,6-Bis(5-bromo-2-furanyl)-2,5-bis(2-octyldodecyl)-2,5-dihydro-pyrrolo[3,4-*c*]pyrrole(2*H*,5*H*)-1,4-dione (0.296 g, 0.3 mmol), 2,5-bis(trimethylstannyl)-thieno[3,2-*b*]thiophene (0.1398 g, 0.3 mmol), and bis(triphenylphosphine)palladium(II) dichloride (7 mg, 0.01 mmol) were dissolved in anhydrous toluene (15 mL) in a 25 mL flask under argon. The mixture was heated to 90 °C and stirred for 48 h under argon to obtain a viscous dark greenish blue solution. A small amount of bromobenzene (0.5 mL) was added to the mixture and stirred at 90 °C for an additional 6 h to react with any unreacted trimethylstannyl end groups. After cooling down to room temperature, the reaction mixture was added dropwise into methanol with stirring (200 mL). The dark solid precipitates were filtered off and washed with methanol. The solid was then transferred to a Soxhlet extraction apparatus and extracted until the extracts were almost colorless with methanol, acetone, and hexane successively. Finally the solid was dried and extracted with chloroform to dissolve the polymer. After evaporating the solvent, dark blue films were obtained (0.290 g, 98.0%). M_w/M_n (GPC) = 346 996/131 961, PDI = 2.63, UV-vis-near IR: 797 nm (in chloroform); 794 nm (thin film).

Fabrication and characterization of OTFT devices

A typical bottom-gate, top-contact OTFT device configuration was adopted to evaluate PDBF-*co*-TT. Heavily *n*⁺-doped Si wafers with a thermally grown silicon oxide layer (~200 nm) were used as substrates to build the OTFT devices. The conductive silicon layer was used as both the gate electrode and the support, while the SiO₂, which has a capacitance of ~17 nF cm⁻², functioned as the gate dielectric. The detailed OTFT fabrication and characterization procedures are similar to the previously reported ones.⁴

Fabrication and characterization of OPV devices

Indium-doped tin oxide (ITO) glass substrates were cleaned, dried and treated with UV-ozone. A layer of PEDOT:PSS (~40 nm) was spin coated on the substrate at 2000 rpm by using a commercial PEDOT:PSS solution (Clevios 4083) and then annealed at 140 °C on a hot plate under nitrogen. The organic semiconductor blend layer was then deposited by spin-coating (at 1500, 2500, or 4000 rpm) a solution of PDBF-*co*-TT and PC₇₁BM in a mixture of chloroform and *o*-dichlorobenzene (4 : 1 by volume) on top of the PEDOT:PSS layer. The first batch of devices had donor–acceptor ratios of 1 : 1, 1 : 2 and 1 : 3 and the total concentration of the semiconductors was 24 mg mL⁻¹. 1,8-Diiodooctane (DIO) or 1-chloronaphthalene (CNp) (0.5, 1, and 2% by volume) was optionally added to the solution as a solvent additive. The second batch of devices had a donor–acceptor ratio of 1 : 2 and the total concentration of semiconductors was 21 mg mL⁻¹. Varied amounts of DIO (0.5, 1, and 2% by volume) were added to the solution. After spin coating, samples were heated on a hot plate at 60 °C for 10 min to remove residual solvent. An aluminium cathode was deposited on top of the polymer blend layer by thermal evaporation

through a shadow mask under a pressure of $\sim 10^{-5}$ mbar to complete the device. The device area is approximately 9 mm^2 .

Characterization of devices was performed under dry nitrogen in a glove box. For a typical device, the external quantum efficiency (EQE) spectrum was measured first, which was conducted by placing the device under a low intensity (~ 0.01 sun) monochromatic, mechanically-chopped (217 Hz) light. The resulting photocurrent signal was detected through a SR830 lock-in amplifier and calibrated against a silicon photodetector with a known EQE. The obtained EQE spectrum was then used to determine the appropriate solar simulator light level for proper AM1.5 simulation, based on the standard spectral mismatch factor method. The photocurrent–voltage curve was measured under the simulated AM1.5 solar illumination using a Keithley 2400 Sourcemeter under dry nitrogen in a glove box.

Conclusions

We designed and synthesized a novel DPP-containing donor–acceptor π -conjugated polymer, PDBF-co-TT, which comprises of (i) a DPP unit as the acceptor building block, (ii) one fused aromatic thieno[3,2-*b*]thiophene as the electron donor, and (iii) two furan units as electron donating bridges. Owing to the highly ordered edge-on polymer chain packing in thin films, strong intermolecular interactions, large π – π overlap, and well-interconnected thin film morphology, PDBF-co-TT exhibited high hole mobility values of up to $0.53 \text{ cm}^2 \text{ V}^{-1} \text{ s}^{-1}$ when used as a channel semiconductor in OTFT devices. This polymer has low-lying HOMO and LUMO energy levels and a small band gap, which are desirable for an electron donor for OPVs. The favoured energy levels and the optimum band gap of PDBF-co-TT helped the attainment of a high open circuit voltage and a high short circuit current. The high hole mobility and good solubility of this polymer semiconductor contributed to the relatively high fill factor, while its low HOMO level resulted in a large open circuit voltage. High power conversion efficiency of 4.38% was achieved for the PDBF-co-TT:PC₇₁BM based solar cell with a proper selection of the donor–acceptor ratio, solvent additive, and spin-coating speed.

Acknowledgements

The work was supported by Agency of Science, Technology and Research (A*STAR), Institute of Material and Research Engineering (IMRE) of Singapore, and the Y. Li's NSERC Discovery Grants provided by the Canadian Government.

Notes and references

- H. Yan, Z. Chen, Y. Zheng, C. Newman, J. R. Quinn, F. Dotz, M. Kastler and A. Facchetti, *Nature*, 2009, **457**, 679.
- H. N. Tsao, D. Cho, J. W. Andreasen, A. Rouhanipour, D. W. Breiby, W. Pisula and K. Müllen, *Adv. Mater.*, 2009, **21**, 209.
- H. N. Tsao, D. M. Cho, I. Park, M. R. Hansen, A. Mavrinskiy, D. Y. Yoon, R. Graf, W. Pisula, H. W. Spiess and K. Müllen, *J. Am. Chem. Soc.*, 2011, **133**, 2605.
- Y. Li, S. P. Singh and P. Sonar, *Adv. Mater.*, 2010, **22**, 4862.
- Y. Li, P. Sonar, S. P. Singh, M. S. Soh, M. M. van and J. Tan, *J. Am. Chem. Soc.*, 2011, **133**, 2198.
- Y. Li, P. Sonar, S. P. Singh, W. Zeng and M. S. Soh, *J. Mater. Chem.*, 2011, **21**, 10829.
- J. S. Ha, K. H. Kim and D. H. Choi, *J. Am. Chem. Soc.*, 2011, **133**, 10364.
- H. Bronstein, Z. Chen, R. S. Ashraf, W. Zhang, J. Du, J. R. Durrant, P. S. Tuladhar, K. Song, S. E. Watkins, Y. Geerts, M. M. Wienk, R. A. J. Janssen, T. Anthopoulos, H. Sirringhaus, M. Heeney and I. McCulloch, *J. Am. Chem. Soc.*, 2011, **133**, 3272.
- P. Sonar, S. P. Singh, Y. Li, Z.-E. Ooi, T.-J. Ha, I. Wong, M. S. Soh and A. Dodabalapur, *Energy Environ. Sci.*, 2011, **4**, 2288.
- J. D. Yuen, J. Fan, J. Seifter, B. Lim, R. Hufschmid, A. J. Heeger and F. Wudl, *J. Am. Chem. Soc.*, 2011, **133**, 20799.
- T. Lei, Y. Cao, Y. Fan, C.-J. Liu, S. C. Yuan and J. Pei, *J. Am. Chem. Soc.*, 2011, **133**, 6099.
- J. Mei, D. H. Kim, A. L. Ayzner, M. F. Toney and Z. Bao, *J. Am. Chem. Soc.*, 2011, **133**, 20130.
- X. Guo, R. P. Ortiz, Y. Zheng, M. G. Kim, S. Zhang, Y. Hu, G. Lu, A. Facchetti and T. J. Marks, *J. Am. Chem. Soc.*, 2011, **133**, 13685.
- Y.-J. Cheng, S.-H. Yang and C.-S. Hsu, *Chem. Rev.*, 2009, **109**, 5868.
- B. C. Thompson and J. M. J. Fréchet, *Angew. Chem., Int. Ed.*, 2008, **47**, 58.
- J. Hou, H.-Yu Chen, S. Zhang, R. I. Chen, Y. Yang, Y. Wu and G. Li, *J. Am. Chem. Soc.*, 2009, **131**, 15586.
- T.-Y. Chu, J. Lu, S. Beaupré, Y. Zhang, J.-R. Pouliot, S. Wakim, J. Zhou, M. Leclerc, Z. Li, J. Ding and Y. Tao, *J. Am. Chem. Soc.*, 2011, **133**, 4250.
- I. McCulloch, M. Heeney, C. Bailey, K. Genevicius, I. MacDonald, M. Shkunov, D. Sparrowe, S. Tierney, R. Wagner, W. Zhang, M. L. Chabinyc, R. J. Kline, M. D. McGehee and M. F. Toney, *Nat. Mater.*, 2006, **5**, 328.
- Y. Li, Y. Wu, P. Liu, M. Birau, H. Pan and B. S. Ong, *Adv. Mater.*, 2006, **18**, 3029.
- H. Pan, Y. Li, Y. Wu, P. Liu, B. S. Ong, S. Zhu and G. Xu, *J. Am. Chem. Soc.*, 2007, **129**, 4112.
- H. H. Fong, V. A. Pozdin, A. Amassian, G. G. Malliaras, D.-M. Smilgies, M. He, S. Gasper, F. Zhang and M. Sorensen, *J. Am. Chem. Soc.*, 2008, **130**, 13202.
- R. Rieger, D. Beckmann, W. Pisula, W. Steffen, M. Kastler and K. Müllen, *Adv. Mater.*, 2010, **22**, 83.
- I. Osaka, T. Abe, S. Shinamura and K. Takimiya, *J. Am. Chem. Soc.*, 2011, **133**, 6852.
- Z. Chen, M. J. Lee, R. Shahid Ashraf, Y. Gu, S. Albert-Seifried, M. Meedom Nielsen, B. Schroeder, T. D. Anthopoulos, M. Heeney, I. McCulloch and H. Sirringhaus, *Adv. Mater.*, 2012, **24**, 647.
- E. Conwell, in *Primary Photoexcitations in Conjugated Polymers Molecular Excitons versus Semiconductor Band Model*, ed. N. S. Sariciftci, World Scientific, Singapore, 1997, ch. 4.
- Y. Zhu, R. D. Champion and S. A. Jenekhe, *Macromolecules*, 2006, **39**, 8712.
- D. M. Leeuw, M. M. J. Simenon, A. R. Brown and R. E. F. Einerhand, *Synth. Met.*, 1997, **87**, 53.
- Y. Cui, X. Zhang and S. A. Jenekhe, *Macromolecules*, 1999, **32**, 3824.
- Y. Li, J. Ding, M. Day, Y. Tao, J. Lu and M. D'iorio, *Chem. Mater.*, 2004, **16**, 2165.
- H. Sirringhaus, P. J. Brown, R. H. Friend, M. M. Nielsen, K. Bechgaard, B. M. W. Langeveld-Voss, A. J. H. Spiering, R. A. J. Janssen, E. W. Meijer, P. Herwig and D. M. de Leeuw, *Nature*, 1999, **401**, 685.
- G. Gu, M. G. Kane, J. E. Doty and A. H. Firester, *Appl. Phys. Lett.*, 2005, **87**, 243512.
- C. A. Lee, D. W. Park, S. H. Jin, I. H. Park, J. D. Lee and B. G. Park, *Appl. Phys. Lett.*, 2006, **88**, 252102.
- J. Veres, S. D. Ogier, S. W. Leeming, D. C. Cupertino and S. M. Khaffaf, *Adv. Funct. Mater.*, 2003, **13**, 199.
- N. J. Yang, C. S. Liao and S. A. Chen, *Adv. Funct. Mater.*, 2010, **20**, 1000.
- J. C. Bijleveld, A. P. Zoombelt, S. G. J. Mathijssen, M. M. Wienk, M. Turbiez, D. M. de Leeuw and R. A. J. Janssen, *J. Am. Chem. Soc.*, 2009, **131**, 16616.

- 36 G. Zhang, Y. Fu, Z. Xie and Q. Zhang, *Sol. Energy Mater. Sol. Cells*, 2011, **95**, 1168.
- 37 C. H. Woo, P. M. Beaujuge, T. W. Holcombe, O. P. Lee and J. M. J. Fréchet, *J. Am. Chem. Soc.*, 2010, **132**, 15547.
- 38 A. P. Zoombelt, S. G. J. Mathijssen, M. G. R. Turbiez, M. M. Wienka and R. A. J. Janssen, *J. Mater. Chem.*, 2010, **20**, 2240.
- 39 J. C. Bijleveld, B. P. Karsten, S. G. J. Mathijssen, M. M. Wienk, D. M. de Leeuw and R. A. J. Janssen, *J. Mater. Chem.*, 2011, **21**, 1600.
- 40 M. C. Scharber, D. Mühlbacher, M. Koppe, P. Denk, C. Waldauf, A. J. Heeger and C. J. Brabec, *Adv. Mater.*, 2006, **18**, 789.
- 41 G. Dennler, M. C. Scharber and C. J. Brabec, *Adv. Mater.*, 2009, **21**, 1323.
- 42 J. Peet, J. Y. Kim, N. E. Coates, W. L. Ma, D. Moses, J. Heeger and G. C. Bazan, *Nat. Mater.*, 2007, **6**, 497.
- 43 C. S. Kim, L. L. Tinker, B. F. DiSalle, E. D. Gomez, S. Lee, S. Bernhard and Y.-L. Loo, *Adv. Mater.*, 2009, **21**, 3110.
- 44 D. D. Nuzzo, A. Aguirre, M. Shahid, V. S. Gevaerts, S. C. J. Meskers and R. A. J. Janssen, *Adv. Mater.*, 2010, **22**, 4321.
- 45 C. V. Hoven, X.-D. Dang, R. C. Coffin, J. Peet, T.-Q. Nguyen and G. C. Bazan, *Adv. Mater.*, 2010, **22**, E63.
- 46 C. R. Osterwald, *Sol. Cells*, 1986, **18**, 269.
- 47 M. Kumada and K. Tamao, *Adv. Organomet. Chem.*, 1968, **6**, 19.
- 48 J. Pommerehne, H. Vestweber, W. Guss, R. F. Mahrt, H. Bassler, M. Porsch and J. Daub, *Adv. Mater.*, 1995, **7**, 551.
- 49 B. W. D. Andrade, S. Datta, S. R. Forrest, P. Djurovich, E. Polikarpov and M. E. Thompson, *Org. Electron.*, 2005, **6**, 11.